Progress of Theoretical Physics, Vol. 121, No. 2, February 2009

Rotational Frequency Dependence of Octupole Vibrations on Superdeformed States in ^{40}Ca

Hiromichi Ogasawara,[1] Kenichi Yoshida,[2] Masayuki Yamagami,[2]
Shoujirou Mizutori[3] and Kenichi Matsuyanagi[2]

[1] *Department of Physics, Graduate School of Science, Kyoto University,*
Kyoto 606-8502, Japan
[2] *Theoretical Nuclear Physics Laboratory, RIKEN Nishina Center,*
Wako 351-0198, Japan
[3] *Department of Human Science, Kansai Women's College, Osaka 582-0026, Japan*

(Received October 26, 2008)

By means of the random phase approximation (RPA) calculation based on cranked deformed Woods-Saxon potential, we investigate how rotational motion affects the properties of octupole vibrations built on superdeformed states in ^{40}Ca. A major structure change of the superdeformed yrast states toward a reflection-asymmetric shape is suggested to take place in the region of angular momentum a little higher than the observed maximum value $16\hbar$, owing to a cooperative effect of octupole vibrational correlation and the rotation-aligned particle-hole excitations from the $f_{7/2}$ to the $g_{9/2}$ shell.

Subject Index: 213

§1. Introduction

In medium and heavy mass regions of nuclei, the effects of rotational motion on octupole vibrations in deformed nuclei have been investigated extensively.$^{1)–3)}$ As reviewed by Butler and Nazarewicz,$^{1)}$ how the octupole instability of the mean field develops as a function of angular momentum is one of the central questions underlying these investigations. An early work on this subject by Neergård and Vogel$^{4)}$ demonstrated the importance of Coriolis force already at low-spin band head states of octupole vibrational bands. In that work, using the particle-rotor model Hamiltonian,$^{5)}$ the Coriolis coupling effects were evaluated between octupole vibrational modes with $K = 0$, 1, 2, and 3, determined at the ground state by means of the random phase approximation (RPA), K being the component of angular momentum along the symmetry axis of the prolately deformed nuclei. In a succeeding paper,$^{6)}$ the importance of accurately evaluating the competition between the rotational alignment of angular momenta of octupole vibrations and that of noncollective two quasiparticle excitations was pointed out. In those works,$^{4),6)}$ the possible change of internal structure of the octupole vibrations with increasing rotational angular momentum was ignored.

The limitation mentioned above was removed in the eighties: It became possible to carry out RPA calculation on the basis of rotating (cranked) shell model;$^{7)}$ it is called “RPA in the rotating frame” or more shortly “cranked RPA”.$^{8)–12)}$ In this approach, single-particle basis is constructed taking into account the rotational motion of deformed mean field, so that microscopic structure change of RPA eigenmodes as a function of the rotational frequency can be investigated. Thus, for negative-parity modes near the yrast line, the importance of competition between octupole correlation energies and energy gain due to alignment of specific single-particle angular momentum associated with high-j orbits like $\mathrm{i}_{13/2}$ and $\mathrm{j}_{15/2}$ was pointed out.13)–15) This is so because such high-j single-particle states are usually involved, as a microscopic ingredient, in octupole vibrations described by RPA.

A breakthrough of the study on the nature of negative-parity excitations near the yrast states was brought about by the discovery of superdeformed rotational bands.16)–20) In such strongly deformed nuclei exhibiting beautiful rotational spectra, one can investigate the competitions mentioned above in a much clean way. Thus, on the basis of the RPA calculation in the rotating frame, Mizutori et al.21),22) and Nakatsukasa et al.23),24) suggested several interesting possibilities of how the rotational alignments of individual single-particle motions and octupole correlations compete in a new situation of superdeformed shell structure. Some of the theoretical predictions were already confirmed by later experiments25)–27) and some await further experiments.

In comparison with medium and heavy mass regions of nuclei discussed above, the properties of octupole vibration in deformed nuclei in lighter mass region are less understood: Collective octupole vibrations are well known also in light nuclei, but they are restricted mainly for spherical nuclei. Instead, the possibility of intrinsic reflection asymmetry has been discussed largely in connection with cluster and molecular structure of $N = Z$ nuclei from ^{12}C to ^{44}Ti (see references cited in Ref. 1)).

Several years ago, a superdeformed (SD) band built on the excited 0^+ state lying at approximately 5.2 MeV in ^{40}Ca was found by Ideguchi et al.28),29) It is characterized by a strongly deformed prolate shape with axis ratio of approximately 2:1 and exhibits a beautiful rotational spectrum from $J^\pi = 0^+$ to 16^+. In view of the fact that the low-angular-momentum portions of the SD bands in heavy nuclei are unknown in almost all cases (except the fission isomers), the observation of rotational band starting from the 0^+ states provides a unique opportunity to study low-frequency collective vibrations built on SD states as a function of angular momentum. It may be possible to observe experimentally such collective modes. For theoretical investigation, the study of ^{40}Ca has additional advantages. First, because the proton and neutron shell structures are essentially the same for such an $N = Z$ nucleus, we can expect that strong coherence takes place between the proton and neutron excitations and brings about an enhanced collectivity of these modes. Second, because the number of particle-hole configurations is smaller than those in heavier nuclei, it may be easier to analyze the competition between the rotational alignment effects of collective octupole and single-particle modes of excitation.

In this paper, we study the possible octupole excitations on the SD states in ^{40}Ca and change of their properties as a function of rotational frequency ω_{rot} by extending the previous RPA calculations30) to include the cranking term associated with the rotating deformed mean field. For this purpose, we construct a new computer code to solve the single-particle states in rotating deformed Woods-Saxon potential in terms of the three-dimensional Cartesian coordinate system. On the single-particle basis thus obtained, we carry out RPA calculation diagonalizing the RPA matrix. The result of calculation suggests that a major structure change of the SD yrast states may take place in the region of angular momentum a little higher than the highest angular momentum $16\hbar$ identified in experiments to date, owing to an interplay between octupole vibrational modes and a rotation-aligned particle-hole excitation from the $\mathrm{f}_{7/2}$ to the $\mathrm{g}_{9/2}$ shell.

In the next section, we briefly summarize the calculational scheme of the RPA in the rotating frame. Because the method itself is well known, we describe only those necessary for discussion on octupole vibrations of present interest. In §3, results of numerical analysis of octupole excitations built on the SD state in ^{40}Ca are presented and discussed.

§2. RPA in the rotating frame

2.1. *Single-particle motion in a rotating deformed Woods-Saxon potential*

Let $\hat{c}_k^\dagger$ and $\hat{c}_k$ denote nucleon creation and annihilation operators in a single-particle state k. By using single-particle wave functions $\varphi_k(\vec{r})$ consisting of two components, $\varphi_{k\sigma}(\vec{r})$ $(\sigma = \pm 1)$, with spin x-components $\frac{\hbar}{2}\sigma$, nucleon creation and annihilation operators at a spatial position $\vec{r}$ are written as

$$\hat{\psi}^\dagger(\vec{r}) = \sum_k \varphi_k^\dagger(\vec{r})\hat{c}_k^\dagger = \sum_k \left(\varphi_{k,+1}^*(\vec{r}),\ \varphi_{k,-1}^*(\vec{r})\right)\hat{c}_k^\dagger, \tag{2·1}$$

$$\hat{\psi}(\vec{r}) = \sum_k \varphi_k(\vec{r})\hat{c}_k = \sum_k \begin{pmatrix}\varphi_{k,+1}(\vec{r})\\ \varphi_{k,-1}(\vec{r})\end{pmatrix}\hat{c}_k. \tag{2·2}$$

We consider the following single-particle Hamiltonian describing independent-particle motion in the axially deformed Woods-Saxon potential that is uniformly rotating with rotational frequency ω_{rot} about the x-axis perpendicular to the symmetry axis (z-axis):

$$\hat{h} = \int \hat{\psi}^\dagger(\vec{r})h(\vec{r},\vec{\nabla})\hat{\psi}(\vec{r})d^3\vec{r} = \sum_{k,k'}\left[\sum_{\sigma,\sigma'}\int \varphi_{k'\sigma'}^\dagger(\vec{r})h_{\sigma'\sigma}(\vec{r},\vec{\nabla})\varphi_{k\sigma}(\vec{r})d^3\vec{r}\right]\hat{c}_{k'}^\dagger\hat{c}_k \tag{2·3}$$

with

$$h(\vec{r},\vec{\nabla}) = \left[-\frac{\hbar^2}{2m}\Delta + V_{\mathrm{WS}}(\vec{r})\right]\mathbf{1} + V_{\mathrm{so}}(\vec{r},\vec{\nabla}) - \omega_{\mathrm{rot}}j_x, \tag{2·4}$$

where $\mathbf{1}$ denotes the unit matrix in the 2×2 spin space, and $V_{\mathrm{WS}}(\vec{r})$ and $V_{\mathrm{so}}(\vec{r},\vec{\nabla})$ represent the axially deformed Woods-Saxon potential and the spin-orbit potential, respectively;

$$V_{\mathrm{WS}}(\vec{r}) = -V_0\left[1+\exp((r-R(\theta))/a)\right]^{-1}, \tag{2·5}$$

$$V_{\mathrm{so}}(\vec{r},\vec{\nabla}) = \frac{i}{2}\hbar^2 q\left(\frac{\partial V_{\mathrm{WS}}(\vec{r})}{\partial\vec{r}}\times\vec{\sigma}\right)\cdot\vec{\nabla}, \tag{2·6}$$

with

$$R(\theta) = R_0(\beta)\left(1 + \sqrt{\frac{5}{4\pi}}\beta P_2(\cos\theta)\right), \tag{2·7}$$

where β is the quadrupole deformation parameter, $P_2(\cos\theta)$ is the second-order Legendre polynomial of $\cos\theta$, and $R_0(\beta)$ is fixed under the condition that the volume enclosed by $R(\theta)$ takes the constant value $\frac{4}{3}\pi r_0^3 A$, A being the mass number. We use the parameters of Ref. 31): $V_0 = 51$ MeV, $r_0 = 1.27$ fm, $a = 0.67$ fm, and $\hbar^2 q = -0.44 r_0^2$.

Because the single-particle Hamiltonian $h(\vec{r}, \vec{\nabla})$ is commutable with the parity transformation $\mathcal{P}$ and the rotation about the x-axis by the angle of π, $\mathcal{R}_x = e^{i\pi j_x/\hbar}$, we can construct simultaneous eigenfunctions of these operators:

$$h(\vec{r}, \vec{\nabla})\varphi_k(\vec{r}) = \varepsilon_k \varphi_k(\vec{r}), \tag{2·8}$$

$$\mathcal{P}\varphi_k(\vec{r}) = \wp_k \varphi_k(\vec{r}), \tag{2·9}$$

$$\mathcal{R}_x \varphi_k(\vec{r}) = \alpha_k \varphi_k(\vec{r}). \tag{2·10}$$

The eigenvalues $\wp_k$ $(= \pm 1)$ and α_k $(= \pm i)$ are called parity and x-signature, respectively. Hereafter, we simply call the latter "signature". Because we choose the quantization axis of intrinsic spin to coincide with the rotation axis (x-axis), we can determine single-particle wave functions such that they satisfy the following reflection symmetries (see Appendix A):32),33)

$$\varphi_{k\sigma}(-x, y, z) = -i\alpha_k \wp_k \sigma \varphi_{k\sigma}(x, y, z), \tag{2·11}$$

$$\varphi_{k\sigma}(x, -y, z) = -i\alpha_k \sigma \varphi^*_{k\sigma}(x, y, z), \tag{2·12}$$

$$\varphi_{k\sigma}(x, y, -z) = \varphi^*_{k\sigma}(x, y, z). \tag{2·13}$$

In diagonalizing the single-particle Hamiltonian, we use three-dimensional Cartesian coordinate mesh representation with box boundary condition.32),33) Owing to the reflection symmetries (2·11)–(2·13), we need to explicitly consider only the octant region in space with $x \geq 0$, $y \geq 0$, and $z \geq 0$. The major reason why we use the coordinate mesh representation is that we intend to apply, in due course, the present approach to neutron-rich unstable nuclei close to the drip line where the continuum plays an essential role. For this aim, the coordinate mesh representation may be better suited in comparison with that in terms of the harmonic-oscillator basis. We also intend to replace, in the future, the Woods-Saxon potential with the Skyrme-Hartree-Fock (SHF) potential.34) The computer program constructed in this work will serve as a first step toward such a self-consistent mean-field approach. In numerical calculation, we take the box size extending approximately 2.5 times of the radius $R(\theta)$ in each direction and the space is discretized with the mesh spacing of 0.6 fm. Numerical reliability with respect to the box size and the mesh spacing was carefully checked by Inakura et al.35) and shown that this choice gives fairly accurate results. Specifically, we take 15 lattice points in the x- and y-directions and 25 lattice points in the z-direction. We use the deformation parameter $\beta = 0.6$ and the same single-particle wave functions for protons and neutrons ignoring the Coulomb potential.

2.2. *Octupole vibrations on rotating superdeformed states*

As a residual interaction for the RPA calculation, we use a density-dependent contact interaction $\hat{v}$ whose matrix elements are given by Ref. 36):

$$v_{k_1'k_2'k_1k_2} = \sum_{\substack{\sigma_1,\sigma_2\\ \sigma_1',\sigma_2'}} \iint \varphi^*_{k_1'\sigma_1'}(\vec{r}_1)\varphi^*_{k_2'\sigma_2'}(\vec{r}_2) v_{\sigma_1'\sigma_1\sigma_2'\sigma_2}(\vec{r}_1,\vec{r}_2)\varphi_{k_1\sigma_1}(\vec{r}_1)\varphi_{k_2\sigma_2}(\vec{r}_2) d^3\vec{r}_1 d^3\vec{r}_2 \quad (2\cdot 14)$$

with

$$v_{\sigma_1'\sigma_1\sigma_2'\sigma_2}(\vec{r}_1,\vec{r}_2) = \left\{ \left[t_0 + \frac{1}{6}t_3\rho(\vec{r}_1)\right]\delta_{\sigma_1\sigma_1'}\delta_{\sigma_2\sigma_2'} + \left[t_0 x_0 + \frac{1}{6}t_3 x_3\rho(\vec{r}_1)\right]\delta_{\sigma_1\sigma_2'}\delta_{\sigma_2\sigma_1'}\right\}\delta^3(\vec{r}_1-\vec{r}_2), \quad (2\cdot 15)$$

where $\rho(\vec{r})$ denotes the nucleon density and $t_0 = -1100$ MeV·fm^3, $t_3 = 16000$ MeV·fm^6, $x_0 = 0.5$, and $x_3 = 1.0$.[36)]

We now introduce creation and annihilation operators of *particle*, $(\hat{a}^\dagger_k, \hat{a}_k)$ and *hole*, $(\hat{b}^\dagger_k, \hat{b}_k)$, defined as

$$\hat{c}^\dagger_k = (1-\theta_k)\hat{a}^\dagger_k + \theta_k\hat{b}_k, \quad (2\cdot 16)$$

$$\hat{c}_k = (1-\theta_k)\hat{a}_k + \theta_k\hat{b}^\dagger_k, \quad (2\cdot 17)$$

where $\theta_k = 1$ when $\varepsilon_k \le \varepsilon_{\rm F}$ (Fermi energy) and 0 otherwise. In terms of these particle and hole operators, the RPA eigenmode creation operators are written as

$$\hat{X}^\dagger_n = \sum_{p,h}(f^n_{ph}\hat{a}^\dagger_p\hat{b}^\dagger_h - g^n_{ph}\hat{b}_h\hat{a}_p), \quad (2\cdot 18)$$

where $\sum_{p,h}$ indicates a summation over particle-hole configurations of both protons and neutrons. We use the index p (h) to specify the particle (hole) states, while the index k is used for general cases. From the linearized equation of motion,

$$[\hat{H},\ \hat{X}^\dagger_n] = \hbar\omega_n\hat{X}^\dagger_n, \quad (2\cdot 19)$$

we obtain eigenvalue equations in matrix form

$$\sum_{p',h'}\begin{pmatrix} A_{php'h'} & B_{php'h'} \\ -B^*_{php'h'} & -A^*_{php'h'}\end{pmatrix}\begin{pmatrix} f^n_{p'h'} \\ g^n_{p'h'}\end{pmatrix} = \hbar\omega_n\begin{pmatrix} f^n_{ph} \\ g^n_{ph}\end{pmatrix} \quad (2\cdot 20)$$

for each sector specified by parity $\wp$ and signature α. In Eq. (2·19), $\hat{H} = \hat{h} + :\hat{v}:$ with $:\hat{v}:$ denoting the normal product of $\hat{v}$ with respect to the particle and hole operators. The matrix elements $A_{php'h'}$ and $B_{php'h'}$ are given as

$$A_{php'h'} = (\varepsilon_p - \varepsilon_h)\delta_{pp'}\delta_{hh'} + \bar{v}_{ph'hp'}, \quad B_{php'h'} = \bar{v}_{pp'hh'}, \quad (2\cdot 21)$$

where $\bar{v}_{k_1'k_2'k_1k_2} = v_{k_1'k_2'k_1k_2}$ when (k_1,k_2) represents a pair of a proton and a neutron while $\bar{v}_{k_1'k_2'k_1k_2} = v_{k_1'k_2'k_1k_2} - v_{k_2'k_1'k_1k_2}$ when (k_1,k_2) corresponds to a pair of identical nucleons. We diagonalize the RPA eigenvalue equation (2·20) treating the rotational frequency $\omega_{\rm rot}$ as a parameter and taking into account all particle-hole configurations with $\varepsilon_p - \varepsilon_h \leq 30$ MeV. It is certainly desirable to check the convergence of numerical results by comparing with calculation using a larger cutoff energy. Because it is computationally demanding, this task is deferred to a future work, however.

We evaluate isoscalar transition amplitudes for octupole operators between the yrast state $|0\rangle$ and the RPA excited states $|n\rangle = \hat{X}_n^\dagger|0\rangle$ as functions of $\omega_{\rm rot}$. The octupole operators are classified in terms of their K values (z-component of angular momentum) and signature α, and denoted as $O^{(K,\alpha)}(\vec{r})$. The signature α is defined as $\mathcal{R}_x O^{(K,\alpha)}(\vec{r})\mathcal{R}_x^{-1} = \alpha O^{(K,\alpha)}(\vec{r})$. Explicitly, they are given as

$$O^{(0,-)}(\vec{r}) = r^3 Y_{3,0}(\theta,\phi), \tag{2·22}$$

$$O^{(K,+)}(\vec{r}) = \frac{i}{\sqrt{2}} r^3 \big[Y_{3,-K}(\theta,\phi) - (-1)^K Y_{3,+K}(\theta,\phi)\big], \quad (K \neq 0) \tag{2·23}$$

$$O^{(K,-)}(\vec{r}) = \frac{1}{\sqrt{2}} r^3 \big[Y_{3,-K}(\theta,\phi) + (-1)^K Y_{3,+K}(\theta,\phi)\big], \quad (K \neq 0) \tag{2·24}$$

where the index ± stands for ±1. The isoscalar transition amplitudes are calculated as

$$\langle 0|\hat{O}^{(K,\alpha)}|n\rangle = \langle 0|[\hat{O}^{(K,\alpha)},\ \hat{X}_n^\dagger]|0\rangle \tag{2·25}$$

$$= \sum_{p,h}(O_{hp}^{(K,\alpha)} f_{ph}^n + O_{ph}^{(K,\alpha)} g_{ph}^n) \tag{2·26}$$

$$\equiv \sum_{p,h} M_{ph}^{(K,\alpha)}, \tag{2·27}$$

where the sum is taken over particle-hole configurations of protons and neutrons, and

$$\hat{O}^{(K,\alpha)} = \sum_{k,k'} O_{k'k}^{(K,\alpha)} \hat{c}_{k'}^\dagger \hat{c}_k \quad \text{with} \quad O_{k'k}^{(K,\alpha)} = \int \varphi_{k'}^\dagger(\vec{r}) O^{(K,\alpha)}(\vec{r}) \varphi_k(\vec{r}) d^3\vec{r}. \tag{2·28}$$

The signs of f_{ph}, g_{ph}, and $O_{ph}^{(K,\alpha)}$ depend on the chosen signs of single-particle wave functions. On the other hand, the relative signs of $M_{ph}^{(K,\alpha)}$ defined above as products of these quantities are uniquely determined. Therefore, relative signs of $M_{ph}^{(K,\alpha)}$ between different particle-hole configurations serve as a good indicator of the coherence among them, and thus we can learn about the collectivity of individual RPA eigenmodes from their properties.

We call the quantities $S_{3K\alpha} \equiv |\langle 0|\hat{O}^{(K,\alpha)}|n\rangle|^2$ "transition strengths", although these are defined in the rotating coordinate frame so that we cannot directly compare these quantities with experimental data. For this, it is necessary to construct wave functions in the laboratory frame by the Bohr-Mottelson approach[5)] or the angular momentum projection method.[37)] This subject is left for a future work, however.

2.3. *Elimination of spurious center of mass modes*

It is well known that, provided the same Hamiltonian is consistently used in the mean-field and the RPA calculations, the spurious center of mass modes appear at zero energy and they are decoupled from other eigenmodes of RPA. This is no longer true for the RPA calculation in the rotating frame, because the cranking term $-\omega_{\rm rot} j_x$ in the Hamiltonian $\hat{H}$ does not commute with the y- and z-components of linear momentum operators. Thus, some recipe to decouple such spurious modes from octupole vibrational modes in deformed nuclei has been proposed.[38] Fortunately, the numerical calculation of Ref. 13) indicates that the center of mass corrections is unimportant for excitation energies and B(E3) values of heavy nuclei (see also Ref. 1)). Thus, instead of trying to achieve exact decoupling of the center of mass modes, we adopt a procedure to eliminate the spurious mixing components from the RPA eigenmodes in the following two steps. First, we note that here are three center of mass modes representing the displacements in the x-, y-, and z-directions and they carry quantum numbers $(K, \alpha) = (1, +1)$, $(1, -1)$, and $(0, -1)$, respectively. Among them, only the $(K, \alpha) = (1, +1)$ mode commutes with the cranking term $-\omega_{\rm rot} j_x$, so that it should appear as a zero-frequency mode even in a rotating frame if a self-consistent mean-field plus RPA calculation is carried out. Because we are using a phenomenological Woods-Saxon potential in place of the self-consistent mean field, this merit of the RPA theory is lost, unfortunately. To remedy this shortcoming, we multiply a common factor λ to the interaction matrix elements $v_{k_1' k_2' k_1 k_2}$ and determine its value for each $\omega_{\rm rot}$ such that the lowest eigenvalue of the RPA matrix in the $\alpha = +1$ sector becomes zero. We can easily identify the spurious modes among solutions of the RPA eigenvalue problem by evaluating the isoscalar dipole transition strength, since it has an extremely large value.

If separation of the spurious modes is perfectly done, the transition amplitudes for the $\hat{x}$-, $\hat{y}$-, and $\hat{z}$-operators should vanish for the octupole excited states of interest:

$$\langle 0|\hat{x}|n\rangle = \langle 0|\hat{y}|n\rangle = \langle 0|\hat{z}|n\rangle = 0. \tag{2·29}$$

In practice, it is difficult to satisfy this condition owing to the small but nonnegligible mixture of the spurious components. Thus, in the next step, we remove such a mixture from the octupole excited states obtained in the RPA calculation "by hand", as for example, in Ref. 39). Namely, we subtract the center of mass components from every RPA excited states $|n\rangle$ in each sector:

$$|n\rangle \longrightarrow \begin{cases} \mathcal{N}_x(|n\rangle - \chi_x \hat{x}|0\rangle) & \text{for} \quad \alpha = +1, \\ \mathcal{N}_{yz}(|n\rangle - \chi_y \hat{y}|0\rangle - \chi_z \hat{z}|0\rangle) & \text{for} \quad \alpha = -1, \end{cases} \tag{2·30}$$

where

$$\mathcal{N}_x = \left[1 - |\chi_x|^2 \langle 0|\hat{x}^2|0\rangle\right]^{-1/2}, \tag{2·31}$$

$$\mathcal{N}_{yz} = \left[1 - |\chi_y|^2 \langle 0|\hat{y}^2|0\rangle - |\chi_z|^2 \langle 0|\hat{z}^2|0\rangle\right]^{-1/2}, \tag{2·32}$$

$$\chi_x = \frac{\langle 0|\hat{x}|n\rangle}{\langle 0|\hat{x}^2|0\rangle}, \quad \chi_y = \frac{\langle 0|\hat{y}|n\rangle}{\langle 0|\hat{y}^2|0\rangle}, \quad \text{and} \quad \chi_z = \frac{\langle 0|\hat{z}|n\rangle}{\langle 0|\hat{z}^2|0\rangle}. \tag{2·33}$$

It is easily seen that this is equivalent to the replacement of the RPA forward and backward amplitudes, (f^n_{ph}, g^n_{ph}), in the following manner:

- For modes with $\alpha = +1$,

$$f^n_{ph} + g^n_{ph} \longrightarrow f^n_{ph} + g^n_{ph} - \frac{\sum\limits_{p',h'} x_{p'h'}(f^n_{p'h'} + g^n_{p'h'})}{\sum\limits_{p',h'} |x_{p'h'}|^2} x^*_{ph}, \tag{2·34}$$

$$f^n_{ph} - g^n_{ph} \longrightarrow f^n_{ph} - g^n_{ph}. \tag{2·35}$$

- For modes with $\alpha = -1$,

$$f^n_{ph} + g^n_{ph} \longrightarrow f^n_{ph} + g^n_{ph} - \frac{\sum\limits_{p',h'} y_{p'h'}(f^n_{p'h'} + g^n_{p'h'})}{\sum\limits_{p',h'} |y_{p'h'}|^2} y^*_{ph}, \tag{2·36}$$

$$f^n_{ph} - g^n_{ph} \longrightarrow f^n_{ph} - g^n_{ph} - \frac{\sum\limits_{p',h'} z_{p'h'}(f^n_{p'h'} - g^n_{p'h'})}{\sum\limits_{p',h'} |z_{p'h'}|^2} z^*_{ph}. \tag{2·37}$$

Here, x_{ph}, y_{ph}, and z_{ph} represent $\langle 0|\hat{x}|ph\rangle$, $\langle 0|\hat{y}|ph\rangle$, and $\langle 0|\hat{z}|ph\rangle$, respectively. After the above replacements, we renormalize them such that new amplitudes satisfy the normalization condition $\sum_{p,h}(|f^n_{ph}|^2 - |g^n_{ph}|^2) = 1$.

§3. Numerical analysis and discussions

3.1. *Dependence of single-particle energies on rotational frequency*

Let us first examine the single-particle energy diagram in the uniformly rotating frame. Figure 1 shows the single-particle energies as functions of the rotational frequency $\omega_{\rm rot}$. We can clearly see the shell gap at $N = Z = 20$ associated with the superdeformed state in ^{40}Ca. An interesting feature seen in this figure is that the single-particle energy of the level labelled [440]1/2 at $\omega_{\rm rot} = 0$ gradually decreases with increasing $\omega_{\rm rot}$ and crosses the Fermi surface at approximately $\omega_{\rm rot} = 2$ MeV/$\hbar$. This indicates that a major structure change of the SD yrast states will occur in the vicinity of the angular momentum corresponding to this rotational frequency. This level originates from the $g_{9/2}$ shell. In the spherical shell model, its energy is much higher but, owing to the superdeformation, it comes down to this position. Its energy further decreases owing to the Coriolis effect. At $\omega_{\rm rot} = 0$, this level is situated at approximately 6 MeV above the Fermi level, so that its aligned angular momentum is estimated to be approximately 6 [MeV] / 2 [MeV/$\hbar$] = 3$\hbar$. In analyzing numerical results of the RPA calculation, we shall focus our attention on the role this level plays.

3.2. *Properties of octupole excitations on SD states in ^{40}Ca*

The results of the RPA calculation for negative-parity excitation modes on the SD yrast states in ^{40}Ca are presented in Fig. 2. In this figure, the RPA excitation

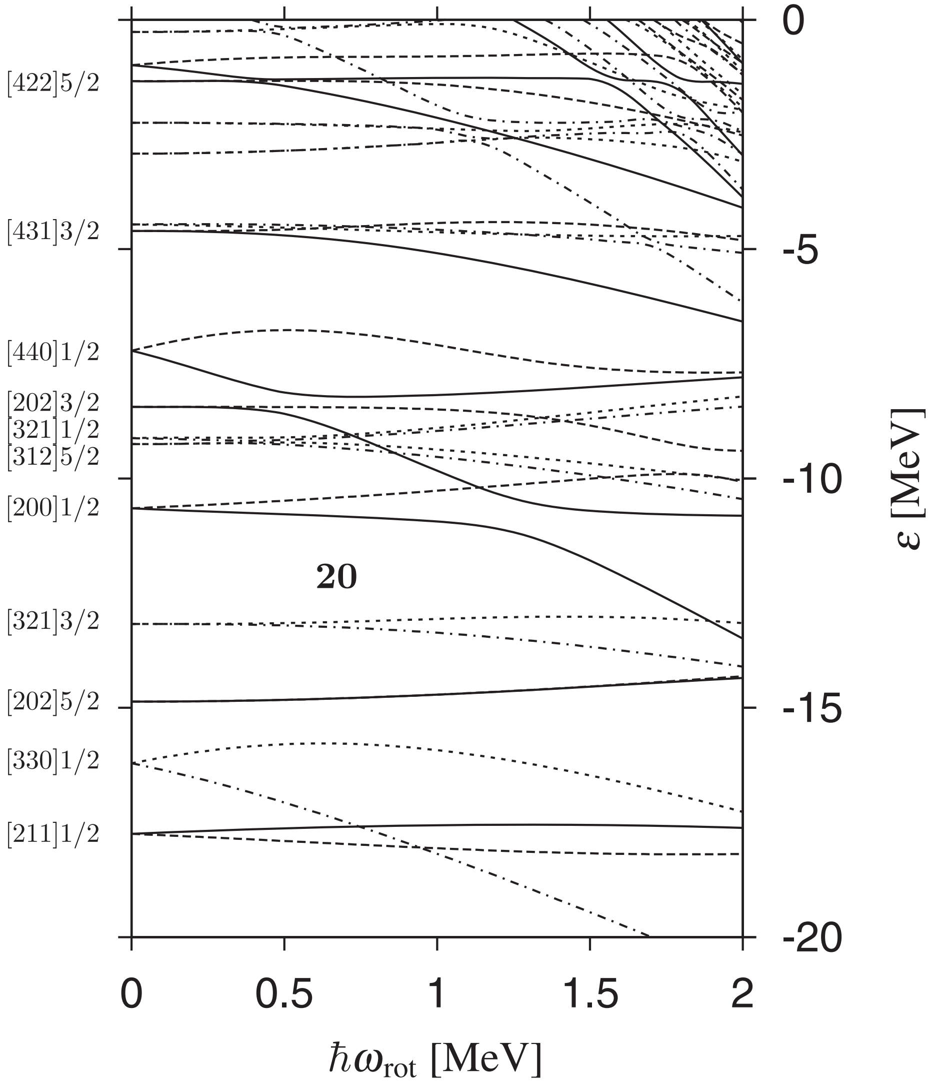

Fig. 1. Single-particle energies ε in the $N = Z$ nucleus ^{40}Ca for the rotating deformed Woods-Saxon plus spin-orbit potentials of Eq. (2·4), plotted as functions of rotational frequency $\omega_{\rm rot}$. The deformation parameter β is fixed at 0.6. Single-particle levels are classified according to the parity ($\wp$) and signature (α) quantum numbers; solid lines for $(\wp, \alpha) = (+1, +i)$, broken lines for $(\wp, \alpha) = (+1, -i)$, dotted lines for $(\wp, \alpha) = (-1, +i)$, and dot-dashed lines for $(\wp, \alpha) = (-1, -i)$. For convenience, they are labelled at $\omega_{\rm rot} = 0$ with asymptotic quantum numbers indicating the largest components of their wave functions. These single-particle energies are used for both protons and neutrons.

energies, the octupole transition strengths S_{30-} $(K = 0)$ and $S_{31\pm}$ $(K = 1)$ for individual RPA modes, and the sum, denoted as $S^{\rm (sum)}_{3K\alpha}$, of individual $S_{3K\alpha}$ values (over the RPA modes with excitation energies less than 5.5 MeV) are plotted as functions of rotational frequency $\omega_{\rm rot}$. Note that there is no positive-signature mode

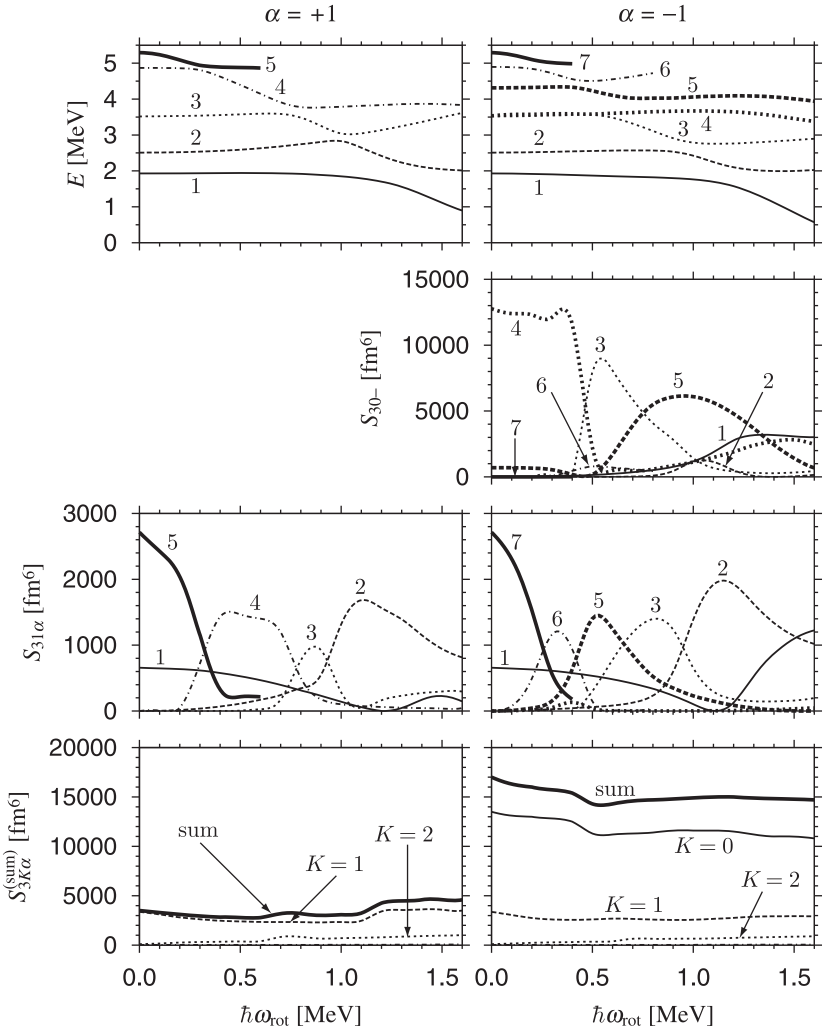

Fig. 2. Results of the RPA calculation for negative-parity excitation modes on the SD yrast states in ^{40}Ca, plotted as functions of the rotational frequency $\omega_{\rm rot}$. Positive-signature excitations are displayed on the left-hand side, while negative-signature excitations on the right-hand side. From the top to the bottom, the RPA excitation energies, the octupole transition strengths S_{30-} ($K = 0$) and $S_{31\pm}$ ($K = 1$) for individual RPA modes, and the sum $S_{3K\pm}^{(\rm sum)}$ of individual $S_{3K\pm}$ values (over the RPA modes with excitation energies less than 5.5 MeV) are plotted as functions of $\omega_{\rm rot}$. The numbers adjacent to individual lines indicate their sequential order according to excitation energy. (On each side, except the bottom panel, line types correspond to individual excitation modes.) The deformation parameter β is fixed at 0.6. Note that there is no positive-signature mode for $K = 0$. Note also that other RPA solutions in the region approximately 5 MeV are not displayed in order to avoid complicating the figure. Continuations of some of the RPA modes of interest are also not shown when they strongly mix with other RPA modes and lose their identities. The S_{31-} strength of the fourth excitation mode is very small so that it is hardly seen in this figure. In the bottom panel, the solid, broken, dotted, and dash-dotted lines indicate the sum $S_{3K\pm}^{(\rm sum)}$ for $K = 0$, 1, 2, and 3, respectively, while the bold-solid line shows the sum of these, $\sum_K S_{3K\pm}^{(\rm sum)}$. The sum $S_{33\pm}^{(\rm sum)}$ is very small so that it is hardly seen in this figure.

for $K = 0$. Because we find no octupole modes with $K = 2$ or 3 possessing a large strength below 5.5 MeV, the transition strengths of individual RPA eigenmodes are shown only for $K = 0$ and 1. This point is reflected in the $S^{(\mathrm{sum})}_{3K\pm}$ values shown in the bottom panels; it is seen that these values for $K = 2$ and 3 are much smaller than those for $K = 0$ and 1.

Let us start the discussion from the case of $\omega_{\mathrm{rot}} = 0$. In this case, signature partners ($\alpha = \pm 1$) with $K \neq 0$ are degenerate in energy. Counting these signature partners as units, we find seven eigenmodes below 5.5 MeV. Among them, the most collective mode is the fourth excitation mode at approximately 3.5 MeV. This mode has $K = 0$ and an extremely large value of octupole transition strength S_{30-}. Note that the Weisskopf unit (W.u.) is approximately 95 fm^6 for ^{40}Ca. Its major microscopic components are the particle-hole excitations [202]5/2 → [312]5/2, [321]3/2 → [431]3/2, and [330]1/2 → [440]1/2 for both protons and neutrons. Another interesting mode is the seventh excitation mode at approximately 5.3 MeV. This mode has $K = 1$ and a large value of $S_{31\alpha}$. It is characterized, in a very good approximation, as particle-hole excitations of protons and neutrons from the single-particle level [321]3/2 to [440]1/2. In comparison to these modes, the octupole transition strength of the first excitation mode at approximately 1.9 MeV is not very large, although it has strength several times of W.u. for $K = 1$. Its major component is the particle-hole excitation from [321]3/2 to [200]1/2. The second excitation mode with $K = 2$ at approximately 2.5 MeV is an almost pure particle-hole excitation from [321]3/2 to [200]1/2. The third excitation mode at approximately 3.5 MeV (which is almost degenerate, in energy, by chance, with the fourth mode discussed above) has $K = 3$. Although it consists of several particle-hole configurations like [321]3/2 → [202]3/2, [202]5/2 → [321]1/2, and [211]1/2 → [312]5/2, its transition strength $S_{33\alpha}$ is very small, because, for each configuration, either the octupole matrix element $O^{(3,\pm)}_{ph}$ or the RPA amplitude f_{ph} is small so that their product $M^{(3,-)}_{ph}$ is small.

It is interesting to note that the particle-hole excitations, like [321]3/2 → [431]3/2, [330]1/2 → [440]1/2, and [321]3/2 → [440]1/2, are the major sources of the large octupole transition strengths of the fourth and seventh eigenmodes. They correspond to the excitation from the $\mathrm{f}_{7/2}$ shell to the $\mathrm{g}_{9/2}$ shell in the spherical j-j coupling shell model. At the spherical shape, the $\mathrm{f}_{7/2}$ shell is unoccupied and the $\mathrm{g}_{9/2}$ shell is situated far above the Fermi surface. The energies of low-Ω single-particle states originating from such high-j orbits markedly decrease owing to the superdeformation, Ω being the component of angular momentum along the symmetry axis of the mean field. It is well known that such high-j shells play an important role in generating low-lying octupole vibrations in both spherical and normal deformed nuclei. However, the particle-hole excitation from the lower high-j shell to the higher high-j shell is a new feature unique to superdeformed states. It is also well known that the response of such high-j orbits to rotational motion is very strong because their Coriolis matrix elements are large. Thus it is interesting to examine how the microscopic structures and properties of the collective octupole vibrational modes change when the rotational frequency ω_{rot} increases, focusing our attention to the fourth and seventh excitation modes.

3.3. *Rotational frequency dependence of the octupole vibrations*

We are particularly interested in the strongly collective $K = 0$ mode that belongs to the negative-signature sector and its interaction with other eigenmodes. By comparing the positive- and negative-signature sectors in Fig. 2, we can imagine that the properties of the $\alpha = +1$ and $\alpha = -1$ octupole excitations with $K \neq 0$ would be similar to each other if the $K = 0$ collective mode and its interactions with other modes were absent. Thus, we focus our attention on the negative-signature sector in the discussion below.

It is immediately seen in Fig. 2 that strong mixings among the RPA modes take place following the variation of $\omega_{\rm rot}$. The most conspicuous trend is that the seventh excitation mode (bold-solid line) quickly comes down in energy and strongly interacts with other modes. The origin of this trend is the rotational alignment of the [440]1/2 ($\alpha = +i$) single-particle state, which is the major ingredient of the seventh mode; owing to the Coriolis coupling effect, its energy quickly decreases as $\omega_{\rm rot}$ increases (see Fig. 1). In the region approximately $\omega_{\rm rot} = 0.5$ MeV/$\hbar$, we see a strong interaction of the collective mode possessing a large $K = 0$ strength S_{30-} with other modes. Note that K is no longer a good quantum number, even approximately, already in this region of $\omega_{\rm rot}$. Namely, these modes contain both the $K = 0$ and 1 components, owing to the Coriolis K-mixing effects. Thus, they exhibit avoided crossing phenomena and exchange their main characters when going through the adiabatic crossing region. Similar avoided crossings successively take place. Accordingly, the octupole transition strengths S_{30-} and S_{31-} are redistributed among these modes, keeping the sum of their strengths for each K approximately constant, as shown in the bottom panel of Fig. 2.

Details of numerical data useful for understanding microscopic structures and properties of collective octupole excitation modes of interest are presented in Figs. 3–6 for some representative cases.

In Fig. 3, the RPA forward and backward amplitudes, f_{ph} and g_{ph}, the unperturbed particle-hole matrix elements of the octupole operator with $K = 0$ and $\alpha = -1$, $O_{ph}^{(0,-)}$ and individual contributions to the RPA octupole transition amplitude, $M_{ph}^{(0,-)}$, are displayed for the fourth excitation mode with $(\wp, \alpha) = (-1, -1)$ at $\omega_{\rm rot} = 0$. Some important particle-hole configurations constituting this mode are also illustrated. Because of the reason mentioned below Eq. (2·28), values of $M_{ph}^{(0,-)}$ are presented with their signs, while absolute values are shown for the other quantities. It is seen that the signs of $M_{ph}^{(0,-)}$ associated with the major configurations denoted A, B, and C are in phase, indicating the collective character of this mode. It is also seen that the particle-hole excitation C, $[330]1/2 \rightarrow [440]1/2$, possesses an extremely large octupole matrix element $O_{ph}^{(0,-)}$ (in absolute magnitude). This excitation mode corresponds to the collective $K = 0$ mode obtained in the mixed representation RPA calculation by Inakura et al.,[35] but its detailed microscopic structure was not clarified in that previous work.

In Fig. 4, the quantities f_{ph}, g_{ph}, $O_{ph}^{(0,-)}$, $O_{ph}^{(1,-)}$, $M_{ph}^{(0,-)}$, and $M_{ph}^{(1,-)}$ are displayed for the sixth excitation mode (dash-dotted line in Fig. 2) with $(\wp, \alpha) = (-1, -1)$ at

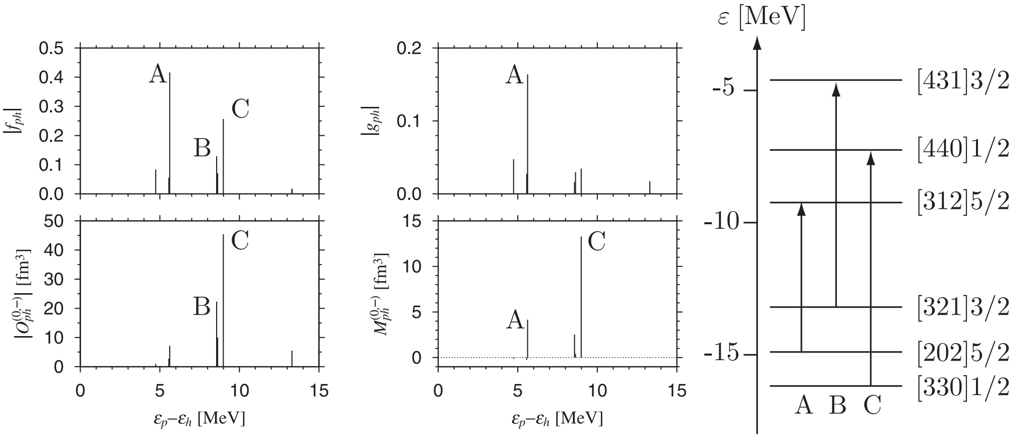

Fig. 3. Microscopic structure of the fourth excitation mode with $(\wp, \alpha) = (-1, -1)$ at $\omega_{\text{rot}} = 0$. The RPA forward and backward amplitudes, f_{ph} and g_{ph}, are shown in the upper-left and upper-middle panels, respectively, while the unperturbed particle-hole matrix elements of the octupole operator with $K = 0$ and $\alpha = -1$, $O_{ph}^{(0,-)}$ and individual contributions to the RPA octupole transition amplitude, $M_{ph}^{(0,-)}$, are displayed in the lower-left and lower-middle panels, respectively, at positions of the abscissa axis representing unperturbed excitation energies, $\varepsilon_p - \varepsilon_h$, of individual particle-hole configurations. Labels A, B, and C indicate some important particle-hole configurations illustrated on the right-hand side. Here, the asymptotic quantum numbers $[N_{\text{osc}}, n_z, \Lambda]\Omega$ are used to label the single-particle levels for convenience. Note that absolute values are shown except for $M_{ph}^{(0,-)}$. Note also that different scales are used for f_{ph} and g_{ph}.

$\omega_{\text{rot}} = 0.4$ MeV/$\hbar$. It is clearly seen that the particle-hole excitation D$_1$, [321]3/2 $(\alpha = -i) \rightarrow$ [440]1/2 $(\alpha = +i)$, is mainly responsible for the large $K = 1$ octupole strength S_{31-} of this mode. This indicates that the sixth excitation mode at $\omega_{\text{rot}} = 0.4$ MeV/$\hbar$ inherits the major component of the seventh excitation mode at $\omega_{\text{rot}} = 0$. At the same time, it is seen that this same configuration carries also the $K = 0$ strength indicating that the Coriolis K-mixing effect is important already at this rotational frequency.

The same quantities are shown in Fig. 5 for the third excitation mode (dotted line in Fig. 2) with $(\wp, \alpha) = (-1, -1)$ at $\omega_{\text{rot}} = 0.8$ MeV/$\hbar$. It is clearly seen that this mode takes over the main characteristics of the sixth excitation mode discussed above at $\omega_{\text{rot}} = 0.4$ MeV/$\hbar$. A remarkable new feature realized at this value of ω_{rot} is a beautiful coherence over many particle-hole configurations. The coherence takes place among almost all $K = 0$ and $K = 1$ transition amplitudes associated with individual particle-hole excitations. Namely, almost all individual contributions, $M_{ph}^{(0,-)}$ and $M_{ph}^{(1,-)}$, exhibited in the bottom panels of this figure take the same sign. This result suggests an interesting possibility that the rotation-aligned high-j particle and the octupole vibrations collaborate to produce a new type of correlation at high angular momentum. It would be interesting to examine this conjecture in a more systematic calculation in the future.

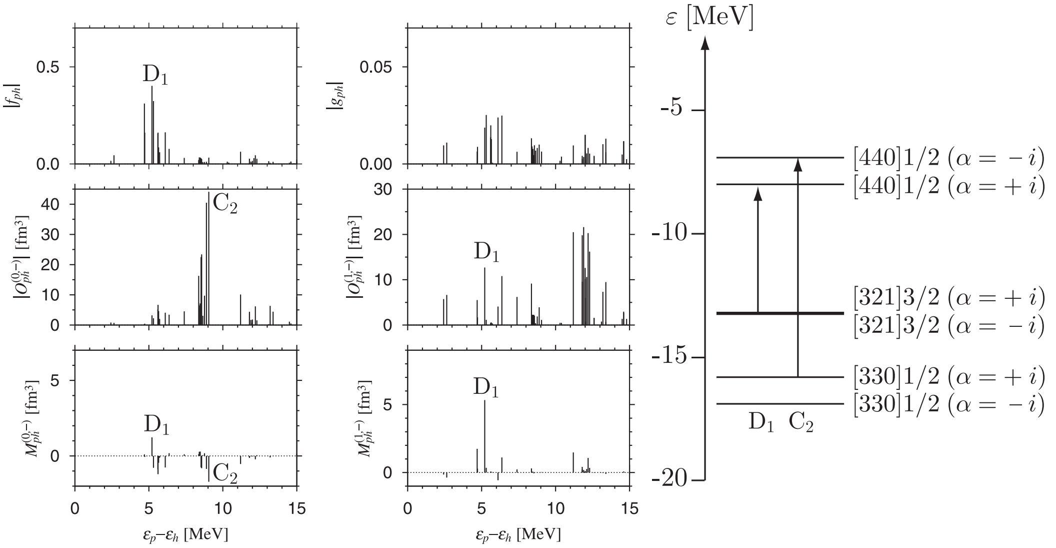

Fig. 4. Microscopic structure of the sixth excitation mode with $(\wp, \alpha) = (-1, -1)$ at $\omega_{\rm rot} = 0.4$ MeV/$\hbar$. In the left part, the RPA forward amplitude f_{ph}, the unperturbed particle-hole matrix elements of the octupole operator with $(K, \alpha) = (0, -1)$, $O_{ph}^{(0,-)}$, and individual contributions to the RPA octupole transition amplitude, $M_{ph}^{(0,-)}$, are displayed in the top, middle, and bottom panels, respectively, at positions of the abscissa axis representing unperturbed excitation energies, $\varepsilon_p - \varepsilon_h$, of individual particle-hole configurations. In the middle part, the RPA backward amplitudes g_{ph}, the matrix elements $O_{ph}^{(1,-)}$, and $M_{ph}^{(1,-)}$ for $(K, \alpha) = (1, -1)$ are shown in a similar fashion. Labels C$_2$ and D$_1$ indicate important particle-hole configurations illustrated on the right-hand side. Here, the asymptotic quantum numbers $[N_{\rm osc}, n_z, \Lambda]\Omega$ are used to label the single-particle levels for convenience. Note that signature partners with $\alpha = \pm i$ (degenerated at $\omega_{\rm rot} = 0$) are split at finite $\omega_{\rm rot}$ (signature splitting). Since the signature splitting of the [321]3/2 level is small, it is hard to see but the configuration D$_1$ involves a hole in the $\alpha = -i$ level. Note also that absolute values are shown except for $M_{ph}^{(K,-)}$ and different scales are used for f_{ph} and g_{ph}.

At $\omega_{\rm rot} = 1.2$ MeV/$\hbar$, as exhibited in Fig. 6, the first excitation mode (solid line in Fig. 2) takes over the major characteristics of the third excitation mode discussed above at $\omega_{\rm rot} = 0.8$ MeV/$\hbar$. We again see the beautiful coherence among many particle-hole configurations indicating the collective character of this mode. Recall that the collectivity of the first excitation mode at $\omega_{\rm rot} = 0$ is much weaker. Namely, the microscopic structure and properties of the first excitation mode are essentially changed in this region of rotational frequency owing to the avoided crossing. Note that, as seen in Fig. 1, the down-sloping [440]1/2 ($\alpha = +i$) level strongly interacts with the [200]1/2 ($\alpha = +i$) level just above the Fermi surface so that the two single-particle wave functions are strongly mixed with each other in this region of rotational frequency. Accordingly, the particle state in the configuration labelled E$_1$ contains an appreciable fraction of the [440]1/2 ($\alpha = +i$) wave function. As seen in Fig. 2, the $K = 0$ octupole transition strength S_{30-} of the first excitation mode gradually increases when $\omega_{\rm rot}$ exceeds 1.0 MeV/$\hbar$, and this mode acquires a sizable fraction of the $K = 0$ strength, which originally resides in the fourth excitation mode at

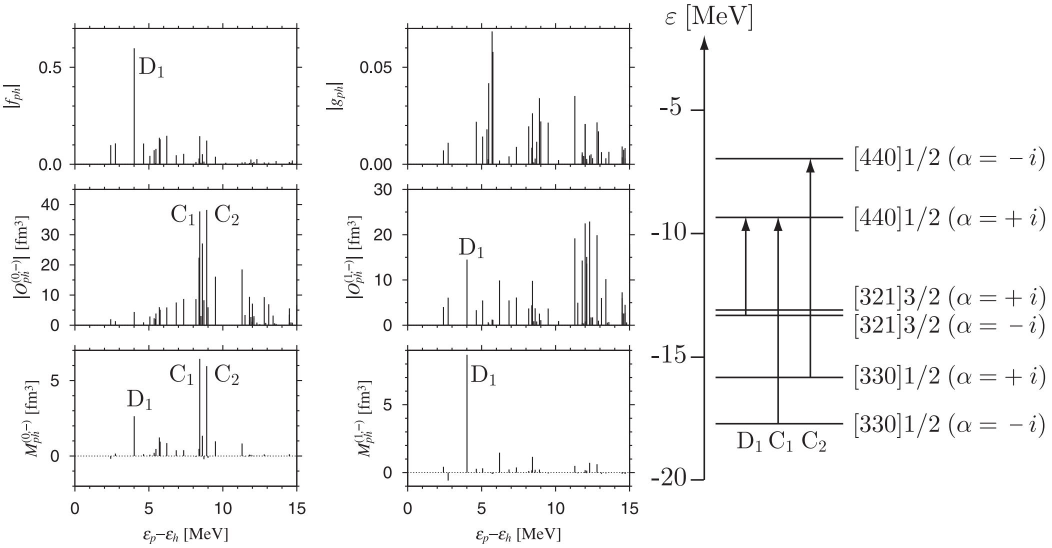

Fig. 5. Same as Fig. 4 but for the third excitation mode with $(\wp, \alpha) = (-1, -1)$ at $\omega_{\rm rot} = 0.8$ MeV/$\hbar$. Labels C$_1$, C$_2$, and D$_1$ indicate some important particle-hole configurations illustrated on the right-hand side.

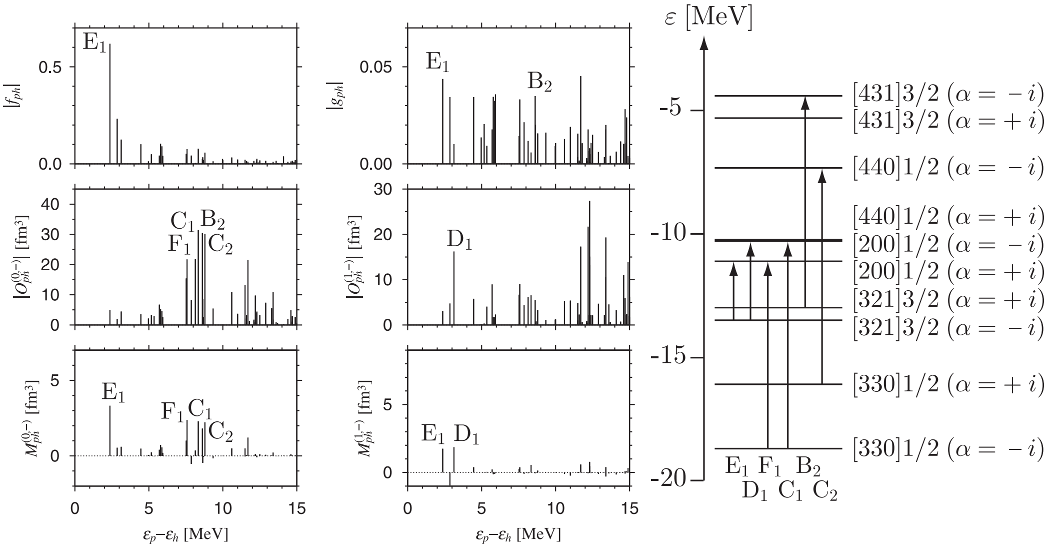

Fig. 6. Same as Fig. 4 but for the first excitation mode with $(\wp, \alpha) = (-1, -1)$ at $\omega_{\rm rot} = 1.2$ MeV/$\hbar$. Labels B$_2$, C$_1$, C$_2$, D$_1$, E$_1$, and F$_1$ indicate some important particle-hole configurations illustrated on the right-hand side. The C$_1$ and D$_1$ configurations both involve a particle in the single-particle level labelled [440]1/2 ($\alpha = +i$).

$\omega_{\rm rot} = 0$.

It is quite interesting to ask what will happen if the rotational frequency is increased further. Unfortunately, we encountered a difficulty in our RPA calculation when the RPA vibrational frequency becomes very small. In such a situation, aside

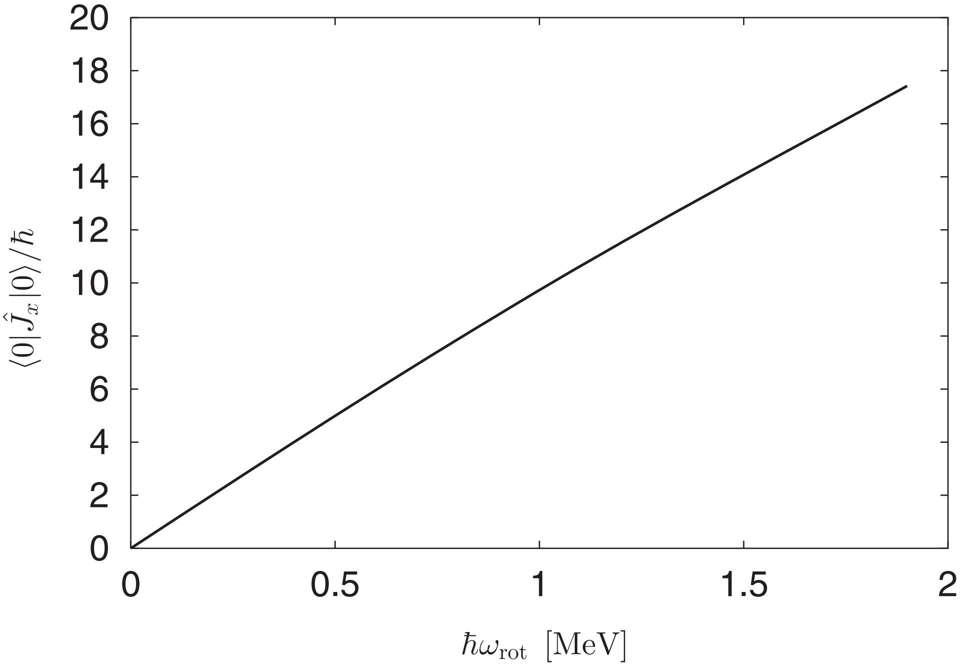

Fig. 7. Expectation value of the angular momentum with respect to the SD yrast states, $\langle 0|\hat{J}_x|0\rangle$, in ^{40}Ca plotted as a function of rotational frequency $\omega_{\rm rot}$. An instability of the axially symmetric SD shape with respect to the octupole vibrational mode is expected to occur beyond $\hbar\omega_{\rm rot} \simeq$ 1.7 MeV, which corresponds to angular momentum approximately $16\hbar$.

from the well-known limitation of the RPA, our recipe (described in §2.3) of approximately eliminating the spurious center of mass mode gradually loses its accuracy and we finally failed to obtain a reliable numerical result for $\omega_{\rm rot} \geq 1.6$ MeV/$\hbar$. A better method of eliminating the spurious components is badly needed, but this task is deferred to a future work. Nevertheless, it seems reasonable to assume that the trend discussed above, which is induced by the rotation-aligned particle (originating from the $g_{9/2}$ shell), will continue. Namely, the energy of the first excitation mode will further decrease and cross the yrast line. This may indicate the occurrence of an instability of the SD shape against the octupole vibration. Then, we would expect that a major structure change of the SD yrast states, like the breaking of reflection symmetry of the mean field, may take place. As shown in Fig. 7, this region of rotational frequency corresponds to angular momentum slightly higher than the maximum value $16\hbar$ so far observed in experiments.[28),29)] The suggested value of the critical angular momentum is a little lower than $24\hbar$ obtained in the symmetry-unrestricted cranked SHF calculation by Inakura et al.[40)] In that work, the nature of the instability occurring at this angular momentum was not clarified.

§4. Concluding remarks

By means of the RPA calculation based on the cranked deformed Woods-Saxon potential, we have investigated how rotational motion affects the properties of octupole vibrations built on SD states in ^{40}Ca. A major structure change of the

SD yrast states toward a reflection-asymmetric shape is suggested to take place in the region of angular momentum a little higher than the observed maximum value $16\hbar$, owing to a cooperative effect of octupole vibrational correlation and the rotation-aligned particle-hole excitations from the $\mathrm{f}_{7/2}$ to the $\mathrm{g}_{9/2}$ shell.

Acknowledgements

We thank T. Inakura for providing us with the result of their SHF and RPA calculation to compare with our calculation result. One of the authors (H. O.) is supported by the Grant-in-Aid for the Global COE Program "The Next Generation of Physics, Spun from Universality and Emergence" from the Ministry of Education, Culture, Sports, Science and Technology (MEXT) of Japan. Another author (K. Y.) is supported by the Special Postdoctoral Researcher Program of RIKEN. The numerical calculations were carried out on supercomputers, NEC SX8 at the Yukawa Institute for Theoretical Physics in Kyoto University and NEC SX8R at the Research Center for Nuclear Physics in Osaka University.

Appendix A

—— *Derivation of Eqs. (2·11)–(2·13)* ——

Equation (2·11) is derived through the following steps:

$$\begin{aligned}\varphi_k(-x,y,z) &= \mathcal{P}e^{i\pi\ell_x/\hbar}\varphi_k(x,y,z) &\text{(A·1)}\\ &= e^{-i\frac{\pi}{2}\sigma_x}\mathcal{P}\mathcal{R}_x\varphi_k(x,y,z) &\text{(A·2)}\\ &= -i\alpha_k\wp_k\sigma_x\varphi_k(x,y,z). &\text{(A·3)}\end{aligned}$$

To derive Eq. (2·13), we note that the eigenvalue equations (2·8)–(2·10) are invariant against the transformation $\mathcal{I}=\mathcal{K}\mathcal{P}e^{i\pi\ell_z/\hbar}$, where $\mathcal{K}$ denotes complex conjugation. The eigenvalues for the transformation $\mathcal{I}$ can take ±1. We then notice that

$$\mathcal{I}\varphi_k(x,y,z)=\varphi_k(x,y,z) \tag{A·4}$$

and

$$\mathcal{I}\{i\varphi_k(x,y,z)\}=-\{i\varphi_k(x,y,z)\} \tag{A·5}$$

are equivalent. Therefore, we can choose the eigenvalue $+1$ without loss of generality. It is easily seen that the left-hand side of Eq. (A·4) is equal to $\varphi_k^*(x,y,-z)$. Thus, Eq. (2·13) follows.

Equation (2·12) is derived in a similar manner:

$$\begin{aligned}\varphi_k(x,-y,z) &= \mathcal{P}e^{i\pi\ell_z/\hbar}e^{i\pi\ell_x/\hbar}\varphi_k(x,y,z) &\text{(A·6)}\\ &= e^{-i\frac{\pi}{2}\sigma_x}\mathcal{K}\mathcal{I}\mathcal{R}_x\varphi_k(x,y,z) &\text{(A·7)}\\ &= -i\alpha_k\sigma_x\varphi_k^*(x,y,z). &\text{(A·8)}\end{aligned}$$

The above derivations are essentially the same, albeit slightly more detailed, as in Refs. 32) and 33).

References

1) P. A. Butler and W. Nazarewicz, Rev. Mod. Phys. **68** (1996), 349.
2) S. Frauendorf, Rev. Mod. Phys. **73** (2001), 463.
3) W. Satuła and R. A. Wyss, Rep. Prog. Phys. **68** (2005), 131.
4) K. Neergård and P. Vogel, Nucl. Phys. A **145** (1970), 33; Nucl. Phys. A **149** (1970), 209; Nucl. Phys. A **149** (1970), 217.
5) A. Bohr and B. R. Mottelson, *Nuclear Structure*, Vol. II (W. A. Benjamin Inc., 1975; World Scientific, 1998).
6) P. Vogel, Phys. Lett. B **60** (1976), 431.
7) R. Bengtsson and S. Frauendorf, Nucl. Phys. A **314** (1979), 27; Nucl. Phys. A **327** (1979), 139.
8) E. R. Marshalek, Nucl. Phys. A **266** (1976), 317; Nucl. Phys. A **331** (1979), 429.
9) D. Janssen and I. N. Mikhailov, Nucl. Phys. A **318** (1979), 390.
10) J. L. Egido, H. J. Mang and P. Ring, Nucl. Phys. A **341** (1980), 229; Nucl. Phys. A **339** (1980), 390.
11) V. G. Zelevinsky, Nucl. Phys. A **344** (1980), 109.
12) Y. R. Shimizu and K. Matsuyanagi, Prog. Theor. Phys. **70** (1983), 144; Prog. Theor. Phys. **72** (1984), 799.
13) L. M. Robledo, J. L. Egido and P. Ring, Nucl. Phys. A **449** (1986), 201.
14) R. G. Nazmitdinov, I. N. Mikhailov and Ch. Briancon, Phys. Lett. B **188** (1987), 171.
15) R. G. Nazmitdinov, Sov. J. Nucl. Phys. **46** (1987), 412.
16) P. J. Nolan and P. J. Twin, Annu. Rev. Nucl. Part. Sci. **38** (1988), 533.
17) S. Åberg, H. Flocard and W. Nazarewicz, Annu. Rev. Nucl. Part. Sci. **40** (1990), 439.
18) R. V. F. Janssens and T. L. Khoo, Annu. Rev. Nucl. Part. Sci. **41** (1991), 321.
19) C. Baktash, B. Haas and W. Nazaerewicz, Annu. Rev. Nucl. Part. Sci. **45** (1995), 485.
20) C. Baktash, Prog. Part. Nucl. Phys. **38** (1997), 291.
21) S. Mizutori, Y. R. Shimizu and K. Matsuyanagi, Prog. Theor. Phys. **85** (1991), 559; Prog. Theor. Phys. **86** (1991), 131.
22) S. Mizutori, T. Nakatsukasa, K. Arita, Y. R. Shimizu and K. Matsuyanagi, Nucl. Phys. A **557** (1993), 125.
23) T. Nakatsukasa, K. Matsuyanagi, S. Mizutori and W. Nazarewicz, Phys. Lett. B **343** (1995), 19.
24) T. Nakatsukasa, K. Matsuyanagi, S. Mizutori and Y. R. Shimizu, Phys. Rev. C **53** (1996), 2213.
25) A. Korichi et al., Phys. Rev. Lett. **86** (2001), 2746.
26) D. Rossbach et al., Phys. Lett. B **513** (2001), 9.
27) T. Lauritsen et al., Phys. Rev. Lett. **89** (2002), 282501.
28) E. Ideguchi et al., Phys. Rev. Lett. **87** (2001), 222501.
29) C. J. Chiara et al., Phys. Rev. C **67** (2003), 041303.
30) K. Yoshida, M. Yamagami and K. Matsuyanagi, Prog. Theor. Phys. **113** (2005), 1251.
31) A. Bohr and B. R. Motteleson, *Nuclear Structure*, Vol. I (W. A. Benjamin Inc., 1969; World Scientific, 1998).
32) P. Bonche, H. Focard, P. H. Heenen, S. J. Kriger and M. S. Weiss, Nucl. Phys. A **443** (1985), 39.
33) P. Bonche, H. Focard and P. H. Heenen, Nucl. Phys. A **467** (1987), 115.
34) M. Bender, P.-H. Heenen and P.-G. Reinhard, Rev. Mod. Phys. **75** (2003), 121.
35) T. Inakura, H. Imagawa, Y. Hashimoto, S. Mizutori, M. Yamagami and K. Matsuyanagi, Nucl. Phys. A **768** (2006), 61.
36) S. Shlomo and G. F. Bertsch, Nucl. Phys. A **243** (1975), 507.
37) P. Ring and P. Schuck, *The Nuclear Many-Body Problem* (Springer, 1980).
38) S. Cwiok, J. Kvasil and B. Choriev, J. of Phys. G **10** (1984), 903.
39) G. Colò, N. Van Giai, P. F. Bortignon and M. R. Quaglia, Phys. Lett. B **485** (2000), 362.
40) T. Inakura, S. Mizutori, M. Yamagami and K. Matsuyanagi, Nucl. Phys. A **710** (2002), 261.